Single Photon Experiments 2023

Tai Xiang

May 3, 2023

Contents

0.1 Summary

0.2 Single Photon Detection Set-up

The basic set-up involves a helium-neon laser in the IR band driven into a BBO crystal. Photons that enter the BBO crystal from the laser undergo spontaneous parametric down-conversion and are then detected within two photon detectors, as shown in figure 1.

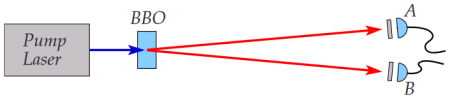

Figure 1: Basic set-up for the SPCM experiment.

Additional beam-splitters can be added between the BBO and the detectors to yield a set-up such as the one shown in figure 2.

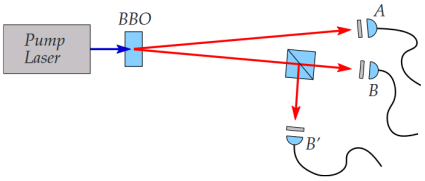

Figure 2: Beam-splitter set-up for the SPCM experiment.

This set-up will be the primary set-up used for the experiments and upgrades listed in the later sections.

0.3 Photon Statistics and Randomness

One of the extensions I explored with the single photon counting module was to apply it to the task of random number generation. Exploiting the quantum intepretation of photons traveling within a beam-splitter and the Poissonian nature of light, a high bitrate random number generator can be developed from the current CCM experimental set-up. The random numbers generated from this set-up can then be used to map out password strings or generate security keys.

With the beam-splitter source of randomness, the set-up generates random bits by observing what detector measures a photon. In the set-up shown in figure 2, a 50–50 beam-splitter is placed between the detector B and B'. In the quantum mechnical interpretation of light, the 50–50 beam-splitter causes an incident photon to have a 50–50 chance of arriving within detector B or B'. Assigning a bit of 0 to B and a bit of 1 to B', we then have a 50–50 chance of getting a bit of 1 or 0. By inserting an additional detector A' that is analogous to B and B', and then adding a 50–50 beam-splitter between A and A', another random bit can be generated.

Furthermore, since photons are emitted from the laser in a Poissonian nature, we can split off a Poissonian distribution fitted to the count of arriving photons, assign buckets to each, and draw random bits in accordance to what bucket a time-step of photon counts falls into. This illustrated in figure 3.

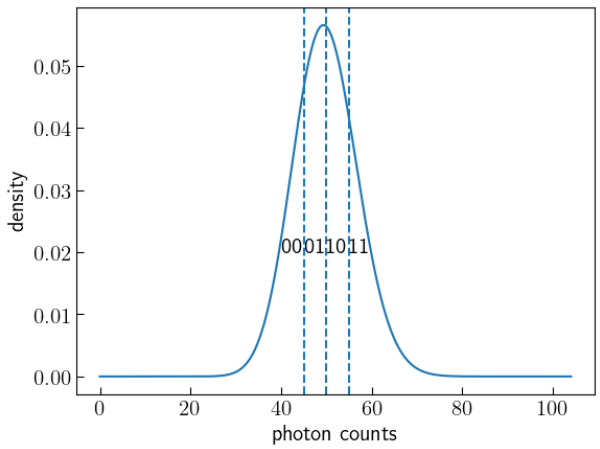

Figure 3: Poissonian distribution segmented into regions of equal area. A bit combination is then assigned to each region.

For example, taking an experiment fitted to the Poissonian displayed in figure 3, if there are 40 incident photons, then we get an output bitstring of 01, if there are 45, we output 01, and so on. A poissonian can be drawn for each detector in the experiment.

In an experiment with two beam-splitters and four detectors utilizing each of the ports available on the SPCM-AQ4C module, a total bitrate of 10 bits per integration time-step can be achieved. In the generation of a password or security key, there are a total of 10 numbers, 40 symbols, 26 lower-case letters, and 26 upper-case letters to choose from, yielding a total of 102 possible selections. A total of 7 bits can reach every single combination of this, with $2^7 - 102 = 28$ additional mappings that are not used and can be overflowed to the next time-step. Each experimental time-step generates 10 bits, so we use 7 to generate a character and overflow the additional 3 bits as well as the additional mappings to the next time-step for efficiency.

We validate the random bits we generate with the NIST statistical test suite for random number generates. The NIST statistical test suite contains a series of tests utilized to determine the randomness of input number sequences. The results of the tests are shown in table 0.3, where a score of 8/10 is considered passing.

Statistical Test	**Proportion**
Frequency	10/10
Block Frequency	10/10
Cumulative Sums	10/10
Longest Run	10/10
Longest Run (Rank)	10/10
Longest Run (FFT)	10/10
NonOverlapping Template	10/10
NonOverlapping Template	9/10
NonOverlapping Template	10/10
NonOverlapping Template	10/10
NonOverlapping Template	9/10
NonOverlapping Template	10/10
NonOverlapping Template	10/10
NonOverlapping Template	10/10
NonOverlapping Template	10/10
NonOverlapping Template	10/10
NonOverlapping Template	10/10
NonOverlapping Template	10/10
NonOverlapping Template	10/10
NonOverlapping Template	8/10
NonOverlapping Template	10/10
NonOverlapping Template	10/10
NonOverlapping Template	9/10
NonOverlapping Template	9/10
NonOverlapping Template	10/10
NonOverlapping Template	10/10
NonOverlapping Template	9/10
NonOverlapping Template	10/10
NonOverlapping Template	10/10
NonOverlapping Template	10/10
NonOverlapping Template	10/10
NonOverlapping Template	10/10
NonOverlapping Template	10/10
NonOverlapping Template	10/10
NonOverlapping Template	10/10
NonOverlapping Template	10/10
NonOverlapping Template	10/10
Random Excursions Variant	10/10

The random numbers generated with our set-up pass the NIST statistical tests. However, although the set-up performs extremely well on these tasks, it should be noted that the passing of statistical tests is not a mathematically rigorous definition of "randomness". The set-up merely performs well on human-defined metrics of randomness.

0.4 Scattering Reduction

An additional improvement I have made to this experimental set-up is the development of multiple schemes to reduce scattering from background noise sources. This section will cover a set of optimizations and developments on this front.

0.4.1 Black Paper and Boxes

A very basic optimization that I performed to reduce scattering was to place long sheets of black paper along the general beam-path of the laser. This was done to ensure scattered light from sources external to the experiment, such as light from the laptop screen and light from the controls of the coincidence counting module, do not interfere with the experiment and generate accidental coincidences.

Additionally, I also added a box that fits the optical components that are along the beam-path prior to the BBO crystal. I cut a small hole that enables the beam to travel into the box and another small hole that enables the beam to exit. Any scattering that arises from the components inside the box is thus contained within it and does not leak out into the room and contaminate the photons arriving at the detectors.

The additional pieces of paper along the beam-path as well as the box enclosure as shown in figure 4.

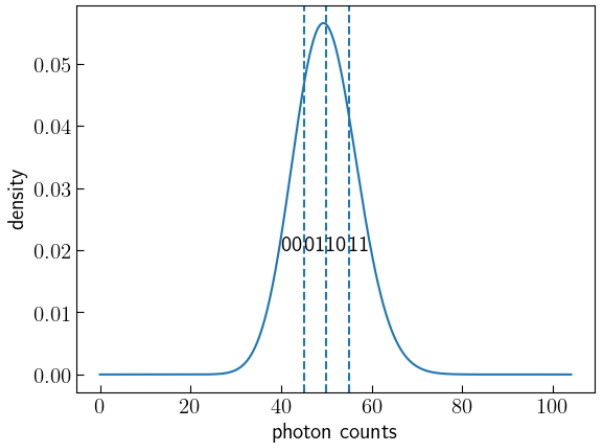

Figure 4: Poissonian distribution segmented into regions of equal area. A bit combination is then assigned to each region.

0.4.2 Enclosures

Another scattering reduction optimization I have made is to create a 3-D printable enclosure for the detectors that reduces the chance of entry for noisey scattered photons. The two-piece enclosure fits and snaps over the detectors and adds a cylindrical nose to the front. The long cylindrical nose reduces the chance of photons that do not arise from the beam-path from hitting the detector. The CAD designs are shown in figure 5.

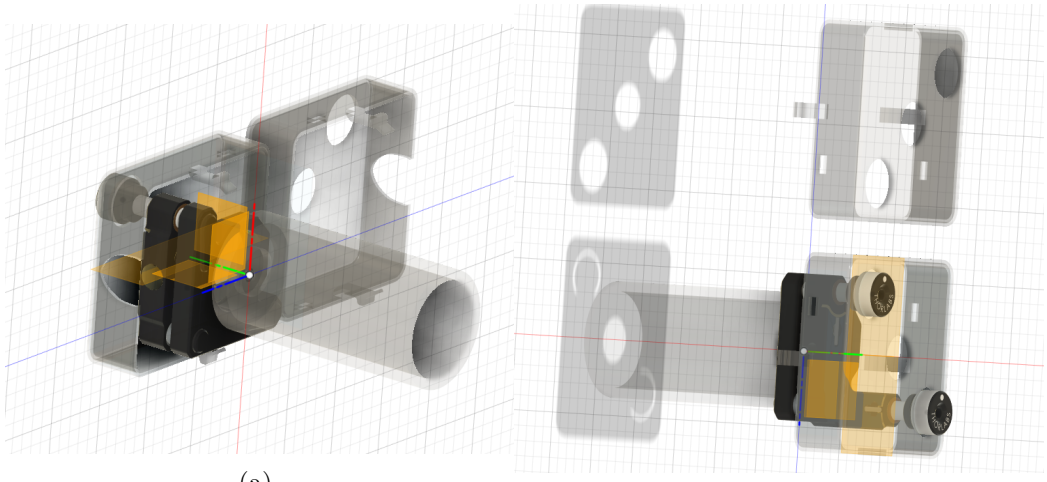

(a) (b)

Figure 5: Figure 5a displays the side view of the enclosure. Figure 5b shows a back view. The two-piece enclosure snaps together through two joints and can easily be taken apart. The cylindrical nose must be glued on to the front of the enclosure.

The cylindrical nose-tube is also designed to fit a filter, such as the FR RG780. When the enclosure was first designed, the ___ filter was used in the experiment. When these optimizations are applied to the basic experimental set-up shown in figure 1, we observe the results shown in figure 6.

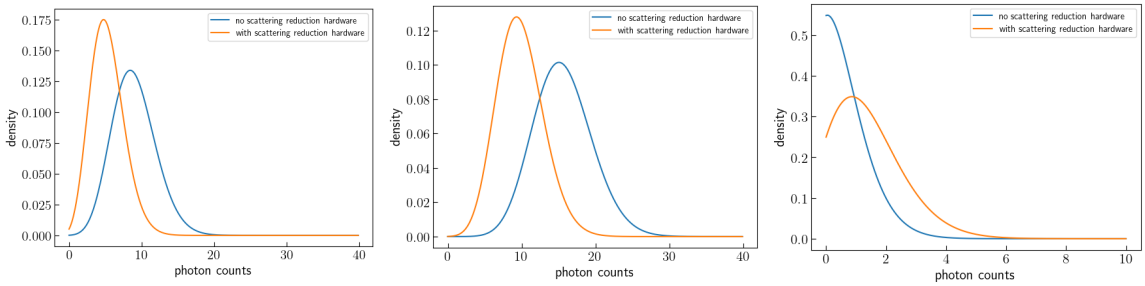

(a) (b) (c)

Figure 6: Figure 6a shows the difference between the Poissonian distribution of photon counts per integration time-step in detector A with and without scattering reduction hardware. Figure 6b shows the difference between the Poissonian distribution of photon counts per integration time-step in detector B with and without scattering reduction hardware. Figure 6c shows the difference between the Poissonian distribution of photon counts per integration time-step in A-B detector coincidences with and without scattering reduction hardware.

We observe that the scattering reduction steps that have been taken cut down on the Poissonian mean of photon arrivals in channel A and B without a major reduction in A–B coincidences. This suggests that the optimizations are cutting out background nose but are not affecting the coincidences generated from down-converted photons (the signal).

0.4.3 Filters

Filters that only enable light in the IR range to pass through are effective in reducing noise, as our laser operates in the IR range. At the beginning of the experiment, we utilized the filters of type *abcd*. An easy optimization we can make to the experiment is to improve the quality of the filter. We test the FR RG780 in place of the *abcd*. The FR RG780 is a longpass filter with a filter profile that is shown in figure 7.

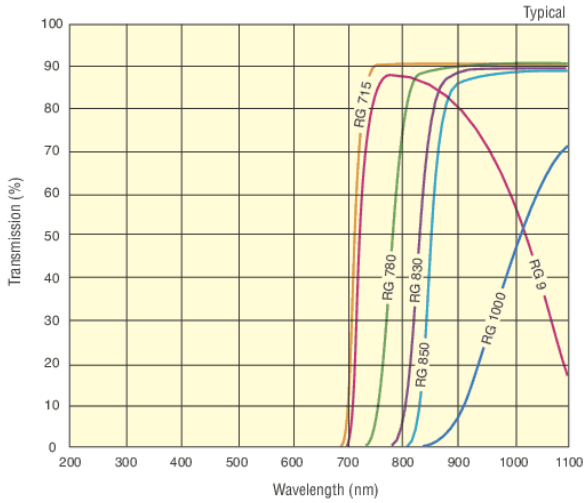

Figure 7: Filter profile of RG780 shown in green.

We compare the results of the experiment with no filter, with the old filters, and with the new RG780 filters. We perform tests with the purple laser, a maglite torch, and an IR LED array.

0.4.4 Laser

For the laser, when analyzing initial counts over time, we observe the results shown in figure 8.

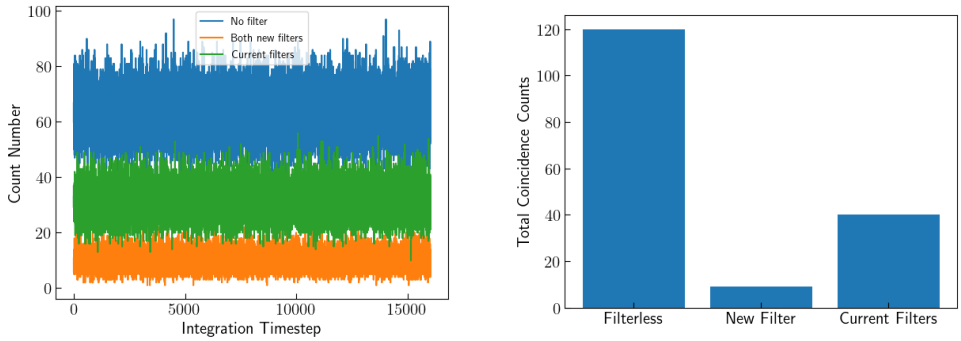

(a) (b)

Figure 8: Figure 8a displays the count numbers measured over each integration timestep for a set-up with no filters, old filters in both the nose tube and following the output optical fiber, and the RG780 filter in both the nose tube and following the output optical fiber. Figure 8b shows the coincidences measured in each configuration.

We observe that the variance in counts go down in accordance to 1 over the shot noise, and we see that the RG780 filter outperforms the current filter in regards to attenuation of the measured count numbers. The coincidence counts also decrease.

Another useful metric we can examine is the α value for each configuration. α is the anticorrelation parameter. For two detectors and a channel for coincidence measurement, we have

$$\alpha_{2d} = \frac{R_c}{R_{acc}^{(2r)}}. \tag{1}$$

Here, R_{acc} denotes the rate of accidental coincidences and is defined to be

$$R_{acc} = 2\tau R_1 R_2 \tag{2}$$

where τ is the coincidence window and R_1 and R_2 denote the count rates for channel 1 and channel 2. R_c denotes the coincidence rate. For correlated sources, such as photon pairs arriving from SPDM, we expect $\alpha > 1$. For an uncorrelated source, such as white light from a torch, we expect $\alpha = 1$.

For each of the filter configurations, we can calculate some α value, finding the results shown in table 0.4.4.

Configuration	α **Value**
No Filters	0.645
Current Filters	0.670
RG780	0.764

Table 1: Table of α values for various filter configurations with a laser photon source.

Curiously, for the laser source, we do not observe an α that is greater than 1, which is what we would expect for a correlated photon source. This defect will be addressed in section 0.5. However, with the new RG780 filter, we achieve a higher α value, indicating that the accidental coincidences from the experiment are decreases and we observe stronger correlation. This suggests that the RG780 filter outperforms our current filters.

0.4.5 Torch

We perform the same set of tests described above with a maglite torch. The torch serves as an uncorrelated photon source, and sends light outwards in a conal shape. We additionally test this configuration to understand how well the new filter performs in the presence of a source that primarily emits photons at a wavelength that is attenuated by the filter.

We once again examine the counts over time and the coincidences measured, though in this test we omit the baseline filter-less case as the counts coming in are too high and excessively compress the axis of our plots. We observe the results shown in figure 9.

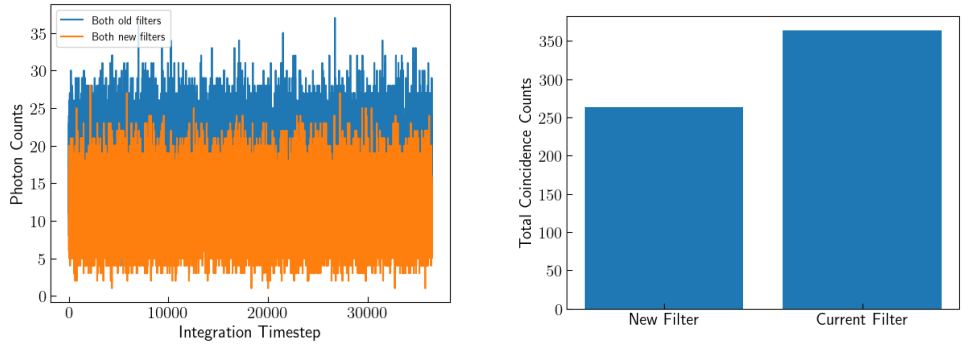

(a) (b)

Figure 9: Figure 9a displays the count numbers measured over each integration timestep for a set-up with old filters in both the nose tube and following the output optical fiber and the RG780 filter in both the nose tube and following the output optical fiber. Figure 9b shows the coincidences measured in each configuration.

Once again, we witness an attenuation in counts and in coincidences. For the case of the torch, we observe the α values shown in table 0.4.5.

Configuration	α **Value**
Current Filters	0.638
RG780	0.677

Table 2: Table of α values for various filter configurations with a torch photon source.

Interestingly, we once again observe results that contradict theory in that our α value is not close to 1. However, we do once again observe that the RG780 filters outperform the current filters in reducing the number of accidental coincidences and yielding a higher α value.

0.4.6 IR LED Array

We also examine the performance of our filters when an IR LED array is placed in front of our detectors. This varies from the torch in that the wavelength of photons emitted by the IR LED is a range the filter does not attenuate but the photon source once again only produces uncorrelated photons. We set-up our IR LED array in accordance with the schematic shown in figure 10.

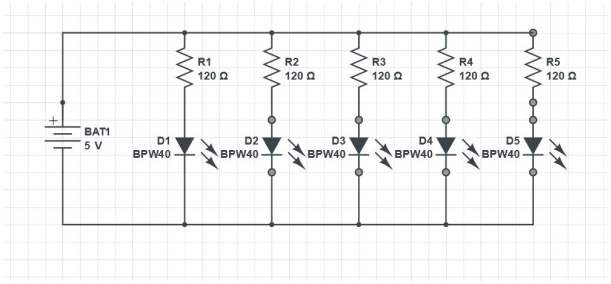

Figure 10: Schematic of IR LED array

We perform the same measurements as those in the above sections and once again omit the filterless detector due to high counts. We observe the results shown in figure 11.

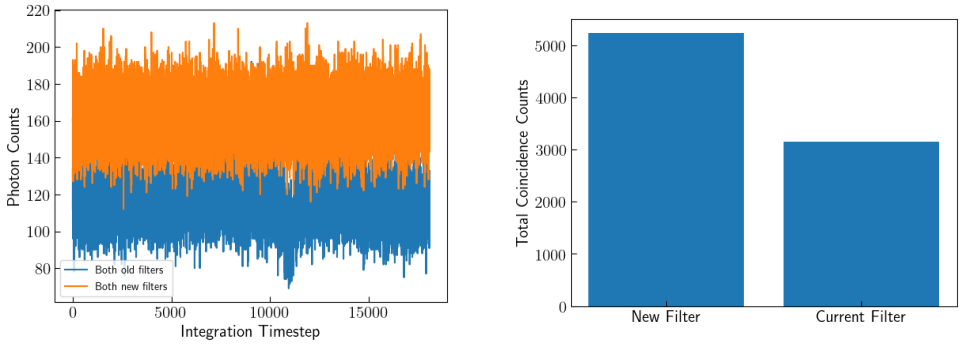

(a) (b)

Figure 11: Figure 11a displays the count numbers measured with the IR LED array set-up over each integration timestep for a set-up with old filters in both the nose tube and following the output optical fiber and the RG780 filter in both the nose tube and following the output optical fiber. Figure 11b shows the coincidences measured in each configuration.

Interestingly, we observe that for the IR LED array, we observe a higher quantity of counts with the RG780 than with the old filters. This suggests that the RG780 filter attenuates the actual signal less, and has a steeper slope at the cutoff 780nm frequency.

When we examine the α values for this set-up, we observe the values shown in table 0.4.6.

Configuration	α **Value**
Current Filters	0.66
RG780	0.63

Table 3: Table of α values for various filter configurations with a torch photon source.

Here, we observe that the RG780 filter yields a lower α value than that of the current filter, suggesting that it measures more accidental coincidences than the current filters. Though this is a negative, the strong cutoff and the high transmission of photons within the signal bandwidth demonstrates that the RG780 is a superior filter than the current filter.

0.5 Defects in Current Coincidence Counting Module (CCM)

In the previous section, we observe a set of measured α values that do not align with theoretical results, namely the measurement of uncorrelated light yields αs on the order of 10^{-1} and the measurement of correlated sources does not yield $\alpha > 1$.

We believe that this result is due to defects in the current coincidence counting module. To further investigate this result, we analyze the pulse-shaper and the channel-by-channel variance of the counter to better understand why this error may arise.

0.5.1 Coincidence Windows and the Pulse Shaper

We first analyze the pulse shaper in the CCM. The pulse shaper alters the waveform of a photon detection event, decreasing the pulsewidths (equivalent to the parameter τ) to those shown in table 0.5.1.

Pulsewidth Setting	**Pulsewidth**
Short	10 $\pm$ 2.5ns
Medium	14 $\pm$ 2.7ns
Long	0.18 $\pm$ 2.8ns
Unaltered	25ns

Table 4: Table of α values for various filter configurations with a torch photon source.

Coincidences are measured by examing waveform overlaps between two detectors, and thus a decrease in pulsewidth may lead to a decrease in accidental coincidences, as two waveforms must arrive within a smaller increment of time for overlap, and subsequently coincidence to occur.

We investigate the α values yielded for different pulsewidths.

Pulsewidth Setting	**Pulsewidth**
Short	0.653
Medium	0.755
Long	0.748
Unaltered	0.930

Table 5: Table of α values for various filter configurations with a torch photon source.

0.5.2 Channel Variance

0.6 Altera DE-2 FPGA CCM